

EFFECT OF SIZE ON THE DESTRUCTION MECHANISMS OF STACKING FAULT TETRAHEDRA INDUCED BY GLIDING DISLOCATIONS IN QUENCHED GOLD—Y. Matsukawa (Argonne National Laboratory), Y. N. Osetsky, R. E. Stoller, and S. J. Zinkle (Oak Ridge National Laboratory)

OBJECTIVE

The destruction processes of stacking fault tetrahedra (SFTs) induced by gliding dislocations were examined by transmission electron microscopy (TEM) in situ straining experiments for SFTs with edge lengths ranging from 10 to 50 nm. At least four distinct SFT destruction processes were identified: (1) consistent with Kimura model for both screw and 60-degree dislocations, (2) stress-induced SFT collapse into a triangular Frank loop, (3) partial annihilation leaving an apex portion, and (4) complete annihilation. Process (4) was observed at room temperature only for small SFTs (~10 nm); however, this process was also frequently observed for larger SFTs (~30 nm) at higher temperature (~853 K). When this process was induced, the dislocation always cross-slipped, indicating only screw dislocations can induce this process.

Introduction

Stacking fault tetrahedra (SFT) are common, sessile, vacancy-type defect clusters in vacancy supersaturated face-centered cubic (fcc) metals having low stacking fault energy like copper, gold, and austenitic stainless steels. The vacancy supersaturation can be introduced by quenching from close to the melting point [1-4] and also by cascade damage due to high energy particle irradiation [5-10]. SFT-dislocation interactions are currently of particular interest as a key mechanism for materials hardening and accompanying ductility reduction of neutron-irradiated fcc metals in nuclear reactor environments [9-16]. An SFT consists of intrinsic stacking faults on four crystallographically equivalent {111} planes locked by six stair-rod dislocations [1,17]. Those sessile stair-rod dislocations act as a strong obstacle against the motion of gliding dislocations responsible for plastic deformation. Also, the complex structure of multiple, interlocked stair-rod dislocations cause the SFT to be highly stable under shear stress. However, defect-free cleared channels (dislocation channels) are commonly observed in the deformation microstructure of both quenched and irradiated metals [12-16,18-22]. This has led to great interest in resolving how SFTs are annihilated during plastic deformation.

The proposed mechanisms for SFT annihilation by gliding dislocations fall into two general categories: 1) annihilation due to the large stress-field associated with nearby dislocations, i.e. SFT destruction by indirect interaction with dislocations, and 2) annihilation due to direct interaction with dislocations. Regarding the first category, Sun et al. and Hiratani et al. used elasticity theory to investigate the stability of an SFT under the stress-field of a nearby dislocation [23-24]. Their calculations showed that the stress-field from a single dislocation could never cause the destruction of SFTs. Regarding the second category, Kimura and Maddin examined conceivable reactions between a gliding perfect dislocation (screw or 60-degree) and the stair-rod dislocations constituting an SFT [25], as described in Fig. 1. Their model predicts that a gliding dislocation can annihilate an SFT if the perfect dislocation dissociates into a pair of Shockley partial dislocations on the surface of the SFT to eliminate the stacking fault. The other three stacking faults in the SFT are then eliminated by a chain reaction starting from the elimination of the first stacking fault.

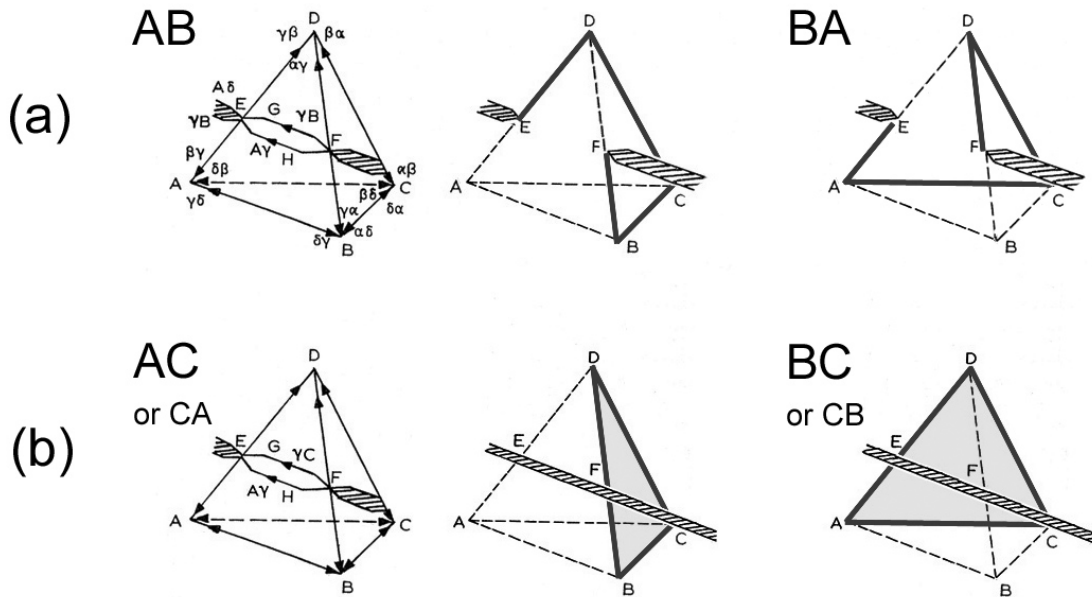


Fig. 1. Kimura's model for SFT destruction induced by direct interaction with (a) a screw dislocation and (b) a 60-degree mixed dislocation [25].

Recent remarkable progress in computer technology has enabled molecular dynamics (MD) computer simulations to investigate the dynamic processes of SFT-dislocation interactions. In 2002, Wirth et al. examined the interaction of a small SFT (~ 2 nm) with edge dislocations in copper [26]. They observed that the SFT remained intact even after multiple (up to six) interactions with a dislocation. SFT destruction took place only when the SFT was initially set up as an imperfect, so-called truncated SFT, which corresponds to an SFT without an apex. Later, Osetsyky et al. examined the interaction of both edge and screw dislocations with larger SFTs up to 10 nm using MD simulations [27-31]. They demonstrated that 1) both edge and screw dislocations could destroy a perfect SFT: the destruction was achieved by the absorption of the major part of the SFT into the dislocations, leaving just the apex of the original SFT. 2) Edge dislocations could destroy SFTs larger than ~ 3 nm (3 nm SFT contains ~ 70 vacancies for copper and ~ 54 vacancies for gold), but there is no such SFT size limitation for screw dislocations. 3) The specimen geometry (whether thin foil or bulk) could affect the final configuration of the screw dislocation after the SFT destruction. However, to date, no MD simulations have reproduced the Kimura's SFT destruction processes where the whole SFT is incorporated into the dislocation (Fig 1(a)) or converted into a triangular Frank loop (Fig 1(b)). The disparity between the Kimura model and simulation results remains unclear. Also, in the simulation-based SFT destruction processes, dislocations absorb only part of the SFT. Annihilation of the whole SFT by an impinging dislocation has not been reported in the MD simulations. This is inconsistent with the fact that numerous experiments reported nothing remains in the cleared channels following deformation in quenched or irradiated materials.

The most direct experimental method to investigate SFT destruction processes involves in situ straining experiments using a transmission electron microscope (TEM). Concurrently with the MD computational research mentioned above, Matsukawa et al. examined the interaction of large SFTs (27-76 nm) with gliding dislocations in quenched gold at deformation temperatures

between 100 K and room temperature [32-35]. They identified various SFT destruction processes including those consistent and inconsistent with Kimura's model. Those inconsistent with Kimura's model involved the process leaving behind an apex of the original SFT, which is quite similar to the simulation-based predictions described above. Shäublin et al. examined small SFTs (~2 nm) introduced into copper by proton irradiation [36]. They observed the formation of elongated debris (a super jog or super kink) on a gliding dislocation upon interaction with an SFT. However, since 2 nm is close to the current TEM resolution limit for diffraction imaging techniques, the detail of the observed process is unclear. Robach et al. examined large SFTs (~90 nm) in quenched gold and small SFTs (~4 nm) in quenched copper [37]. They observed the conversion of those SFTs into different configurations; however, the obtained micrographs were unclear in terms of the detailed morphology of those configurations.

Those preceding TEM results are not comprehensive mainly due to the difficulty of the experiments. The straining stages are in many cases single-tilt, which often prevents the capture of clear images for informative model constructions. More systematic and comprehensive TEM results are desired for a complete understanding of SFT-dislocation interaction processes. Such experimental results are necessary for proper comparison with and validation of atomic-scale MD simulations, which are essential inputs of mesoscopic-scale computer simulations such as dislocation dynamics [38-39]. In this report, we present the results of systematic in situ TEM experiments on the SFT size dependence of SFT destruction processes in gold. The examined SFT edge lengths (referred to as "sizes" in the following) were 10~50 nm, which encompass the size range where direct comparison with MD results can be made. Also, the SFT size range examined in the present study brackets the critical size in an SFT's stability. A previous elasticity theory calculation indicates that SFTs larger than 26.5 nm are energetically meta-stable whereas smaller SFTs are stable compared to faulted vacancy loops throughout the comparison of energy hierarchy between an SFT, a triangular Frank loop, and a truncated SFT [40]. In a comparison between an SFT and a circular Frank loop, the critical size below which the SFT is the stable configuration was reported to be ~10 nm [5].

Experimental Procedure

SFTs were introduced into 99.9975% pure polycrystalline gold specimens, whose thickness was 100 μm , by quenching from 1273 K in an open vertical furnace to 233 K in a CaCl_2 solution. The specimens were kept at 1273 K for 1-30 min in the furnace, and then at 233 K for 10 min in the quenched-in solution. Longer annealing time at 1273K resulted in larger SFTs. The tensile specimens had a rectangular shape (10 mm x 2.5 mm x 100 μm), and the central portion was electro-polished using a twin jet method. The electrolytic polishing solution was a KCN 67 g/l water solution, and the polishing temperature was 276 K. The TEM accelerating voltage was 200 kV, which introduces negligible irradiation damage into gold. The specimen stage was a GATAN Model 671 single-tilt cooling straining stage, whose crosshead speed is variable ranging from 0.01 to 1.00 $\mu\text{m/s}$. In the present observation, the velocity of dislocations was 10-100 nm/s, which is roughly ten orders of magnitude slower than the dislocation velocity in MD simulations [35] (see also Appendix). The motion pictures of SFT-dislocation interaction processes were captured with a GATAN Model 622 camera, at a frame rate of 30 frames/s, recorded on DV tapes, and then computer processed into sequential images. The in situ straining experiments were carried out at room temperature. The SFT-dislocation interaction processes at higher temperatures (~873 K) were observed using GATAN Model 628 single-tilt heating stage. Dislocations glided without applying external stress during heating. The dislocation motion was driven by local specimen bending due to thermal-softening.

SFT Destruction Processes Observed in In Situ TEM Experiments

As addressed in our preliminary report [32], the SFTs introduced by quenching exhibit perfect

pyramidal shape without any truncation [41-44]. Hence, the following descriptions of the destruction processes induced by gliding dislocations are valid for perfect SFTs, as opposed to truncated or imperfectly formed SFTs [26,37].

SFT Destruction Processes Consistent with the Kimura Model

We observed SFT destruction processes consistent with Kimura's model for both screw and 60-degree dislocation interactions. Figure 2 shows the SFT destruction processes leaving multiple super jog segments on the impinging dislocation. In this figure the beam direction was close to $\langle 001 \rangle$, where the SFT appears square in shape. This process was confirmed at all SFT sizes (10~50 nm) without any significant difference in the configuration of multiple super jogs. Figure 3 is a sketch of the configuration of multiple super jog segments in the Kimura model for screw dislocation interactions seen from the $\langle 001 \rangle$ direction. These configurations are consistent with the experimental results: Fig. 2(a) corresponds to Fig. 3(c), and Figs. 2(b) and 2(c) correspond to Fig. 3(a). Those multiple super jogs consist of 60-degree and edge components. Although each segment is glissile, the multiple segments together are practically sessile due to their complicated configurations: in our experiments these super jog dislocations did not glide. In Fig. 2(a), a segment of the gliding dislocation, indicated by the arrow, cross-slipped prior to the interaction with the SFT. This is consistent with Kimura's assumption that this process is induced by a screw dislocation. Since the Kimura model is based on a simple summation of the Burgers vectors of the dislocations, the exact position of dislocation interaction with the SFT should not be a critical factor for inducing these destruction processes (the place of interaction does not affect the sum of the Burgers vectors). However, we never observed the configurations of multiple super jog segments shown in Figs. 3(b) and 3(d). The Kimura mechanism for screw dislocation interaction was induced only when dislocations impinged on SFTs near their base triangle.

Figure 4 shows the SFT destruction process that leaves behind a triangular Frank loop. The beam direction was close to $\langle 001 \rangle$, where the shape of a triangular Frank loop can be readily distinguished from an SFT. The SFT size was 19 nm. After the leading dislocation in a dislocation queue collapsed the SFT into a triangular Frank loop (corresponding to the 95.93 sec frame), the subsequent dislocations interacted with the triangular Frank loop (the 140.53 sec frame). The slip planes of those dislocations are parallel to each other. This indicates that the residual Frank loop was on a plane nonparallel to the glide-plane of the dislocation that destroyed the SFT, which is consistent with Kimura's model for a 60-degree dislocation interaction.

More interactions were seen leaving super jogs than Frank loops since most of the observed interactions involved screw dislocations: Fig. 4 is the only example clearly identified as the Kimura process for a 60-degree dislocation interaction among ~30 observed SFT-dislocation interactions: the process shown in Figs. 1 and 3 in our previous report [35] is categorized in the variant addressed in the following section rather than the Kimura process for 60-degree dislocation. This tendency is consistent with in situ straining experiments carried out by other investigators on gold [1], copper [18,22], and nickel [19-20]. For in situ straining experiments using wedge-shaped thin foil specimens, dislocations were, in many cases, generated at the specimen edge and followed by crack initiation. Those cracks were, in many cases, out-of-plane mode-III shear cracks, as shown in Fig. 5(a). The two areas across the crack were accompanied with thickness fringes, indicating that the crack propagated with significant thickness reduction, which is induced only by out-of-plane shear. Screw dislocations compensate the out-of-plane shear displacements of mode-III cracks as shown in Fig. 5(b), whereas edge dislocations compensate mode-II in-plane shear. Screw dislocation activity is more dominant, presumably because the out-of-plane shear was favorable due to the unique specimen geometry having less of a constraint force in the thickness direction.

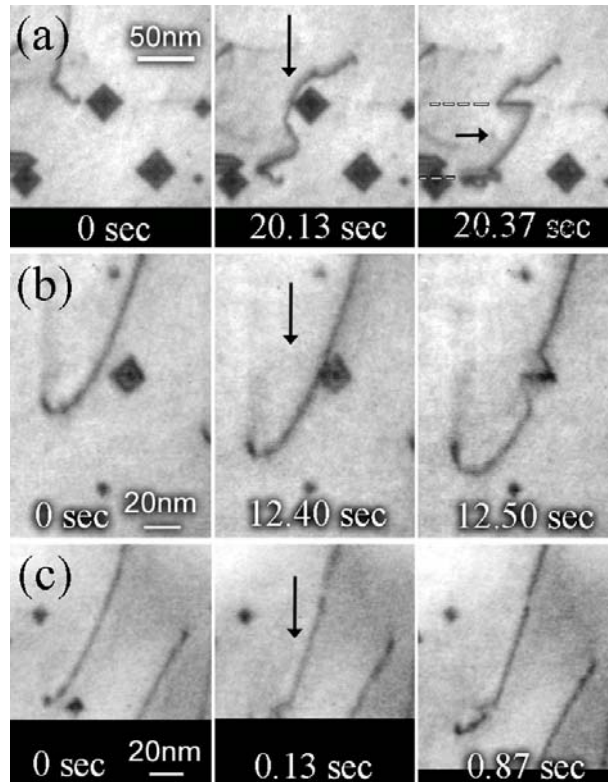


Fig. 2. SFT destruction process at room temperature leaving multiple super jog segments on the impinging dislocation: consistent with the Kimura model for SFT destruction by a screw dislocation. The SFT size was (a) 46, (b) 21, and (c) 12 nm, respectively.

Stress-induced SFT Collapse into a Triangular Frank Loop

Figures 6 and 7 are also SFT destruction processes leaving behind a triangular Frank loop; however, they are different from the Kimura model. The beam direction was close to $\langle 001 \rangle$ for Fig. 6 and $\langle 112 \rangle$ for Fig. 7, and the SFT size was 37 nm for Fig. 6 and 52 nm for Fig. 7. In contrast to Fig. 4, after the leading dislocation in a dislocation queue collapsed the SFT into a triangular Frank loop, the subsequent dislocations never interacted with the triangular Frank loop indicating that the Frank loop was lying on a plane parallel to the glide-planes of those dislocations. In the Kimura model for a 60-degree dislocation, the Frank loop must form on the planes nonparallel to the glide plane of the incident dislocation, as shown in Fig. 1. Large SFTs ($> \sim 37$ nm) always collapsed in this manner when they interacted with the leading dislocation in a dislocation queue.

Large SFTs are energetically meta-stable [5,40], where it is more favorable to transform into a lower energy configuration, i.e. a Frank loop. Accordingly, this transformation would be a stress-induced SFT collapse via an inverse Silcox and Hirsch mechanism [1] due to high stress from a dislocation pile-up. Note that the impinging dislocation is slightly bent when it induces this collapsing process (the 0.97 sec frame in Fig. 6). This indicates that the stress-induced SFT collapse process occurs when the dislocation is in physical contact with the SFT.

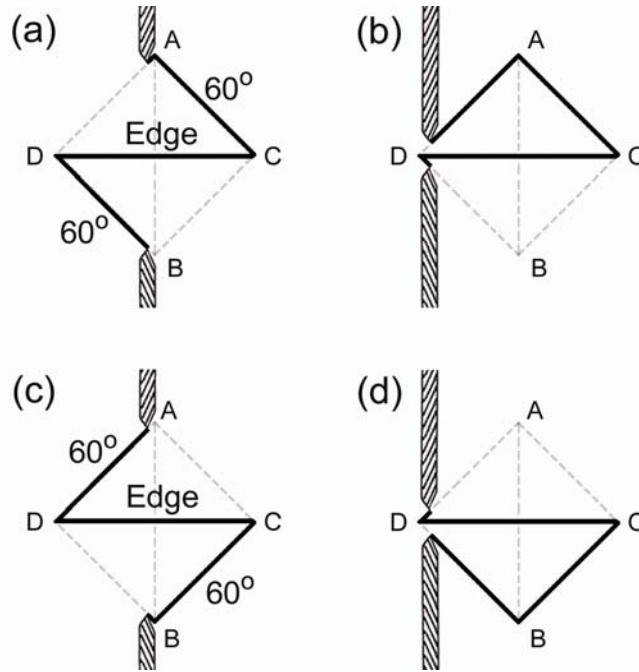


Fig. 3. Configuration of multiple super jog segments assumed in the Kimura model for a screw dislocation, seen from the [001] zone axis: (a) when the Burgers vector $b = \overline{BA}$ and dislocation impingement is near the base triangle ABC , (b) when $b = \overline{BA}$ and dislocation impingement is near the apex D , (c) when $b = \overline{AB}$ and impingement is near the base ABC , and (d) when $b = \overline{AB}$ and impingement is near the apex D .

The smallest SFT that we confirmed that collapsed via this process was 37 nm. SFTs larger than this size always collapsed via this process upon interacting with the leading dislocation in a dislocation queue. Considering that this process was not confirmed for an SFT of 34 nm [33,35], it is highly possible that a critical size is located between 34 and 37 nm. The critical size above which SFTs are meta-stable was estimated to be roughly 26.5 nm in an elasticity theory calculation previously reported by Jøssang and Hirth [40,45]. The discrepancy with the present results may be because Jøssang and Hirth used 55 mJ/m^2 for the stacking fault energy of gold in their calculations whereas more recent values as low as 32 mJ/m^2 have been reported [45].

Partial Annihilation of an SFT Base Leaving a Small SFT

Occasionally, a gliding dislocation destroyed a large SFT leaving behind a small SFT. The small SFT corresponds to the original SFT's apex: the dislocation absorbs only the base portion. This SFT destruction process is rather complicated due to three variants regarding the configuration of the impinging dislocation after the destruction of the SFT, as previously reported elsewhere: 1) formation of sessile segments on the dislocation (super jogs on screw dislocations) [32,34-35], 2) glissile segments (super jogs on edge dislocations) [33], and 3) no super jog segments [33,35].

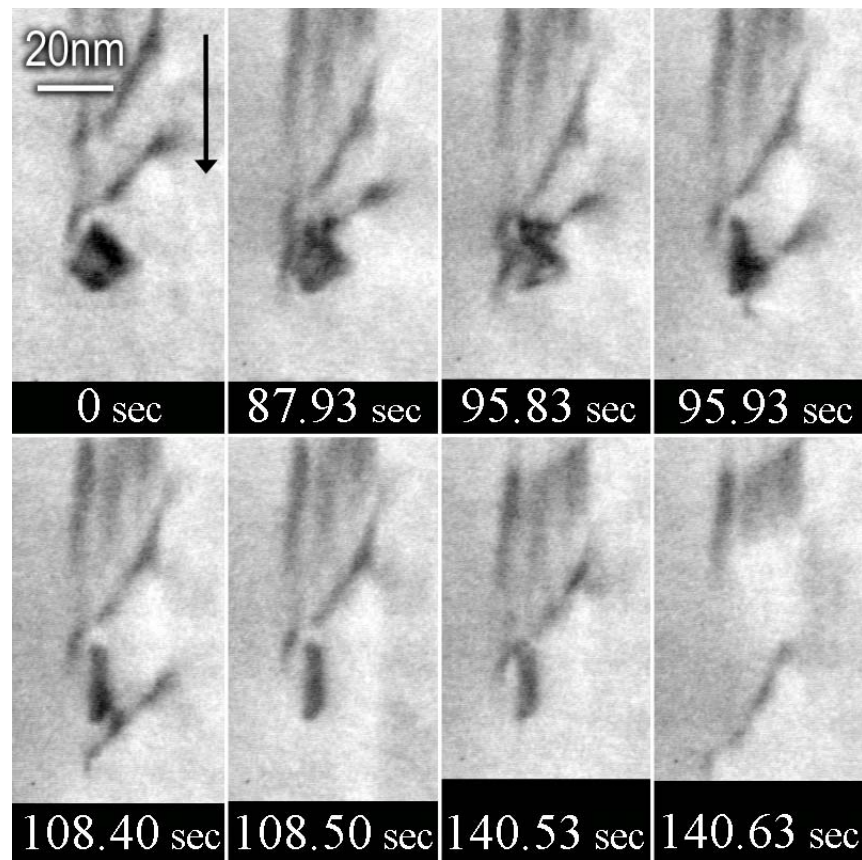


Fig. 4. SFT destruction process leaving behind a triangular Frank loop, consistent with the Kimura model for a 60-degree dislocation. The conversion from an SFT to a triangular Frank loop is captured in the 95.93 sec frame. The Frank loop was finally removed by the following dislocations. The initial SFT size was 19 nm.

Figure 8 shows an example of the case where sessile super-jog segments are created on the impinging dislocation. The size of the original SFT and the remnant small SFT is 26 nm and 5 nm, respectively. The sessile segments formed on the second dislocation in the dislocation queue. Since those segments pinned the dislocation, it inevitably encountered the following dislocations as deformation proceeded. Surprisingly, the sessile segments were transferred from one dislocation to another through dislocation-dislocation interaction. The position and morphology of the sessile segments were unchanged but the segments could transfer to adjacent dislocations within the queue. The dislocations released from the sessile segments were then glissile. To the best of our knowledge, this is the first experimental result that shows the sessile super-jog segments can be transferred among dislocations.

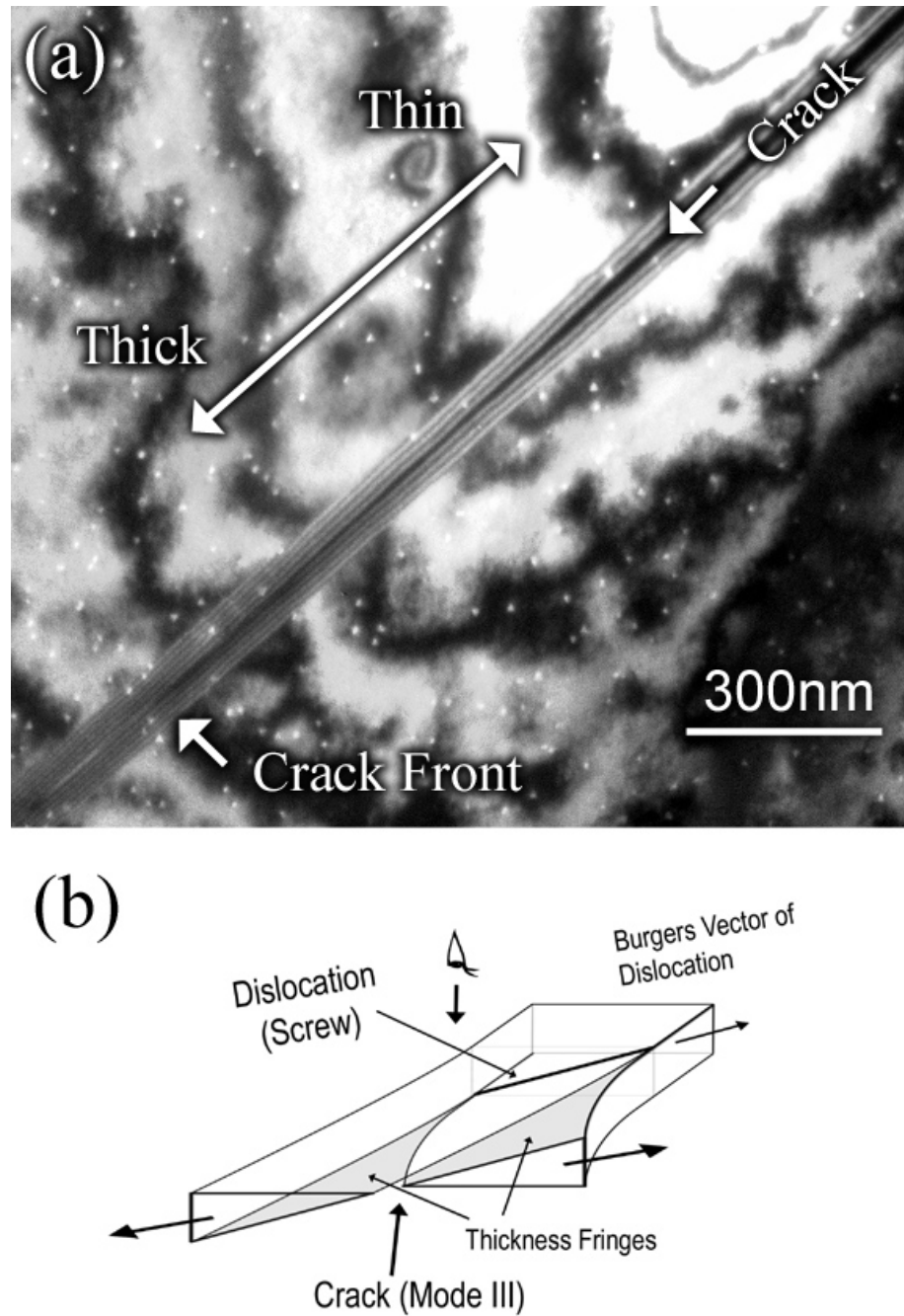


Fig. 5. (a) Typical example of a crack initiated at the specimen edge. Thickness fringes are clearly identified along the crack in the two fractured pieces, indicating that this is a mode-III out-of-plane shear crack. (b) Schematic diagram of the mode-III crack: screw dislocations compensate the out-of-plane shear displacements.

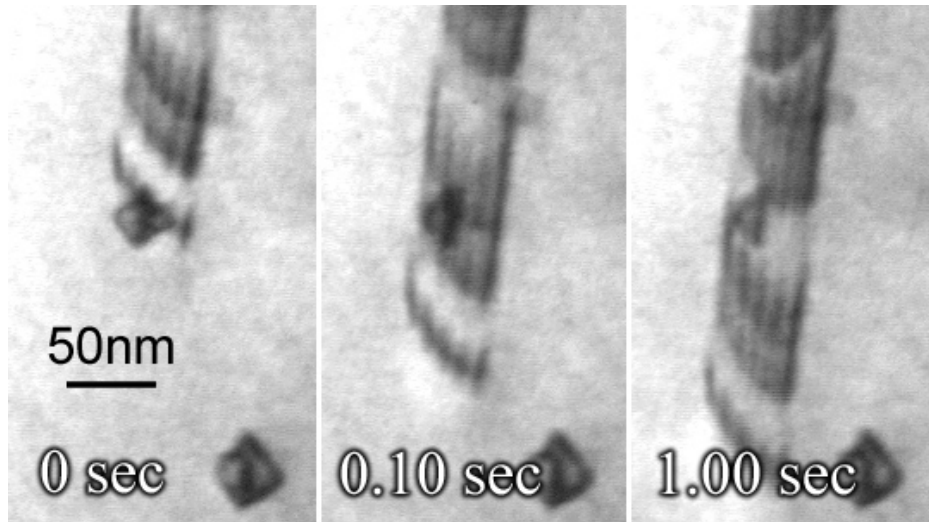


Fig. 6. SFT destruction process leaving a triangular Frank loop, inconsistent with the Kimura model for a 60-degree dislocation. After the first dislocation collapsed the SFT to a triangular Frank loop, the following dislocations never interacted with the Frank loop. This indicates the Frank loop was lying on a plane parallel to the glide plane of those dislocations, which is inconsistent with the Kimura model. The initial SFT size was 37 nm and the observation direction was near [001].

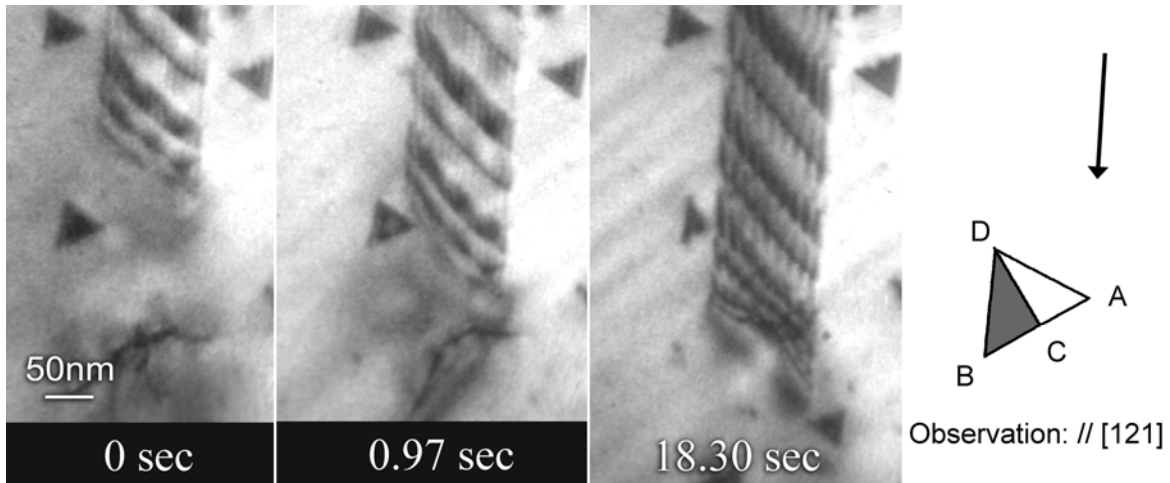


Fig. 7. Same SFT destruction process as Fig. 6 but observed from [121]. The initial SFT size was 52 nm.

Figure 9 shows an example of the case leaving no sessile/glissile segments on the impinging dislocations. The leading dislocation (indexed as A) in a dislocation queue destroyed an SFT (31 nm). No jog segments were confirmed on the dislocation after the SFT destruction (at 7.57 sec). The dislocation finally glided away, leaving surface traces unparallel to the surface traces of previous motion. This indicates that the whole dislocation A cross-slipped, indicating that this is a screw dislocation. A small SFT (~5 nm) remained where dislocation A interacted with the original SFT. The following Shockley partial dislocations indexed as B constricted immediately after the disappearance of dislocation A: the constriction is conjectured to be induced by a stress

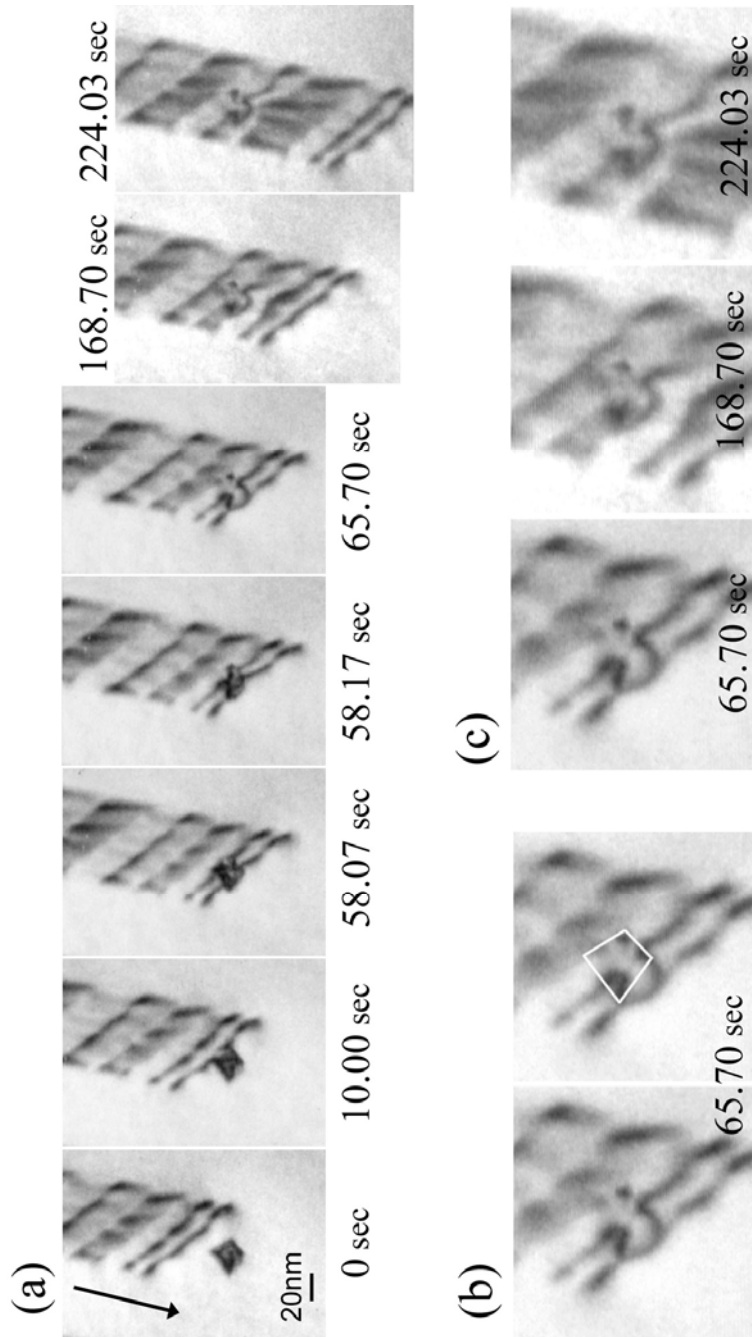


Fig. 8. SFT destruction process leaving behind an apex portion of the SFT and sessile segments on the impinging dislocation. The SFT original size and the remnant apex portion were 26 and 5 nm, respectively. After the SFT destruction by the first and second dislocations, sessile segments formed on the second dislocation. When the second dislocation interacted with the trailing dislocations, the sessile segments were transferred to those dislocations. The leading dislocations that released the sessile segments could then glide as usual.

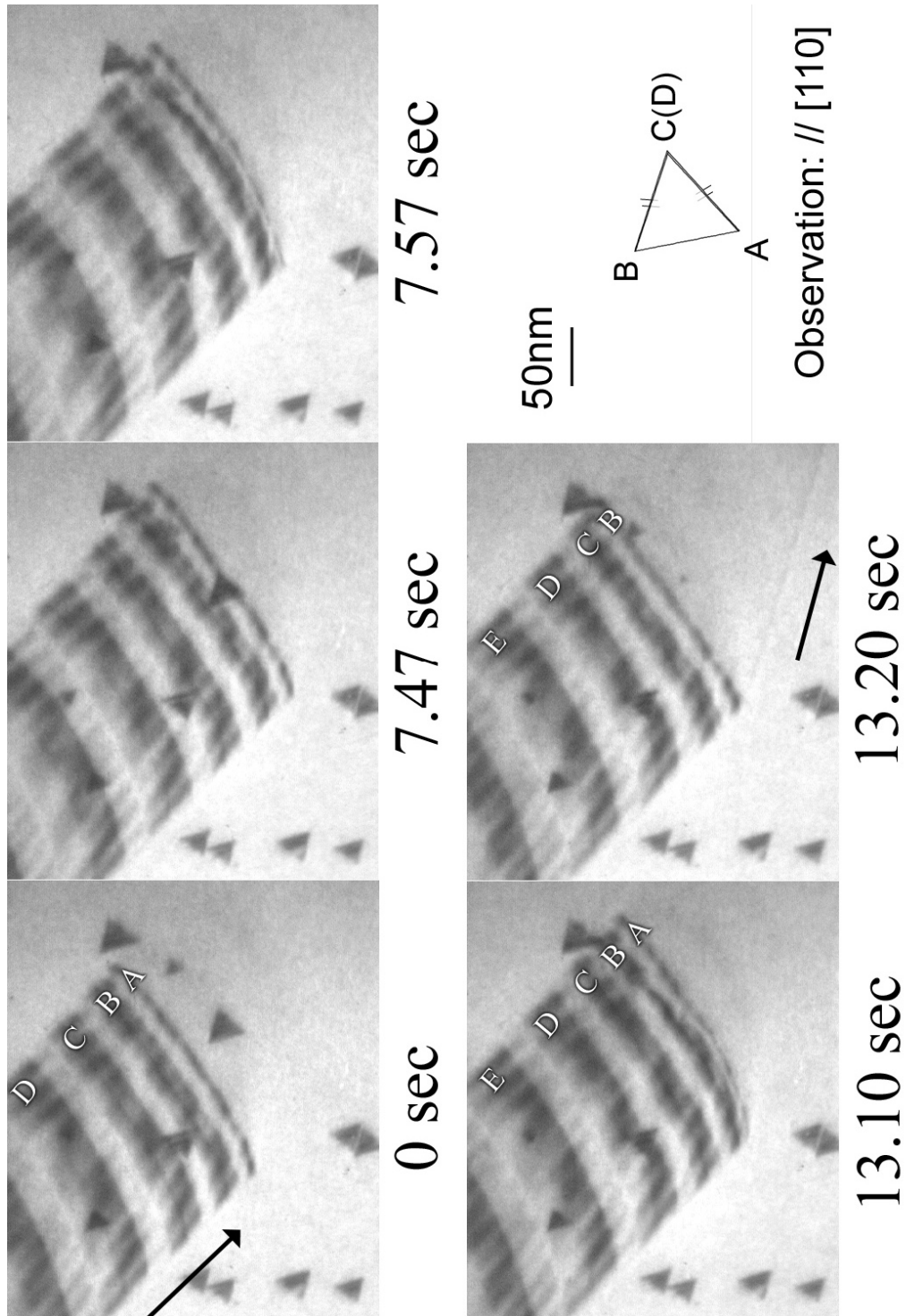


Fig. 9. SFT destruction process leaving behind an apex of the SFT and no sessile segments on the dislocation. The SFT size and the remnant apex were 31 and 5 nm, respectively. After the SFT destruction, the dislocation glided away on a slip plane different from the original plane via cross-slip.

concentration at the front of the dislocation queue. Exactly the same feature was confirmed in another example that we previously reported [33,35]: upon the annihilation of the SFT base portion, the dislocation glided away on a different slip plane from the original plane via cross-slip.

Figure 10 shows a different case where dislocation segments are not observed following destruction of the SFT base. After the annihilation of an SFT (11 nm) leaving behind the 5 nm apex portion, the dislocation continued to glide on the same slip plane as before the interaction with the SFT. Therefore, cross slip to another glide plane does not always occur when destruction of the SFT base occurs without super jog formation.

Complete SFT Annihilation without any Remnants

Figure 11 shows an example of complete SFT annihilation leaving no remnants and no sessile segments on the impinging dislocation. This process is important especially for understanding the formation mechanism of cleared channels, because the other SFT destruction processes leave some remnants or sessile segments on the impinging dislocation whereas nothing remains in cleared channels. In Fig. 11, one of two ends of the dislocation line intersected by specimen surfaces moved away from the trace of previous locus upon annihilation of the 11 nm SFT. This indicates that the whole dislocation cross-slipped rather than having local cross-slip as seen in the Kimura model for a screw dislocation (Figs. 2 and 3). This process was frequently observed for small SFTs (~10nm) at room temperature and never observed for larger SFTs.

At high temperature (~873K) SFT destruction without any visible remnants was the dominant SFT annihilation process even for large SFTs, as shown in Fig. 12 (SFT size: 30 nm). This is understandable considering the fact that cross-slip can occur more easily at higher temperatures.

The SFT destruction processes observed in the present TEM in situ experiments fall into four categories, as summarized in each section: (3.1) Kimura processes, (3.2) stress-induced SFT collapse, (3.3) apex remnant, and (3.4) no remnants. To date we have observed roughly 30 SFT destructions induced by dislocations for a wide range of SFT sizes (10~>50 nm): most of the results were obtained at room temperature and a few of them at 100 K [35] and 873 K. Process (3.1) was confirmed at all SFT sizes (at least the one for a screw dislocation) at room temperature and 100 K. Process (3.2) occurred for SFTs larger than 34 nm at room temperature and 100 K. Process (3.3) was confirmed at all SFT sizes at room temperature. Process (3.4) occurred only for small SFTs (~10 nm) at room temperature but frequently occurred for larger SFTs (~30 nm) at 873 K.

Judging from the remnant type, process (3.3) would appear to be essentially the same process as found in MD models. Formation of super jog segments was not confirmed in Fig. 9 and Fig. 10. In this situation, MD simulations have indicated that the dislocation should exhibit a double cross-slip. However, such a double cross-slip was not detected in Fig. 9 or Fig. 10. In Fig. 10, although the dislocation appeared to continue to glide on the same plane, this may be regarded as a double cross-slip onto a plane near the original slip plane. In Fig. 9, the dislocation exhibited only a single cross-slip, which is inconsistent with MD results. Process (3.4) may also be regarded as a variant of the MD models if remnant size was small (a few angstroms) invisible to TEM observation. However, this process was also achieved by a single cross-slip. These results indicate that a double cross-slip of the whole dislocation is not necessary: a partial/complete SFT annihilation was achievable by a single cross-slip.

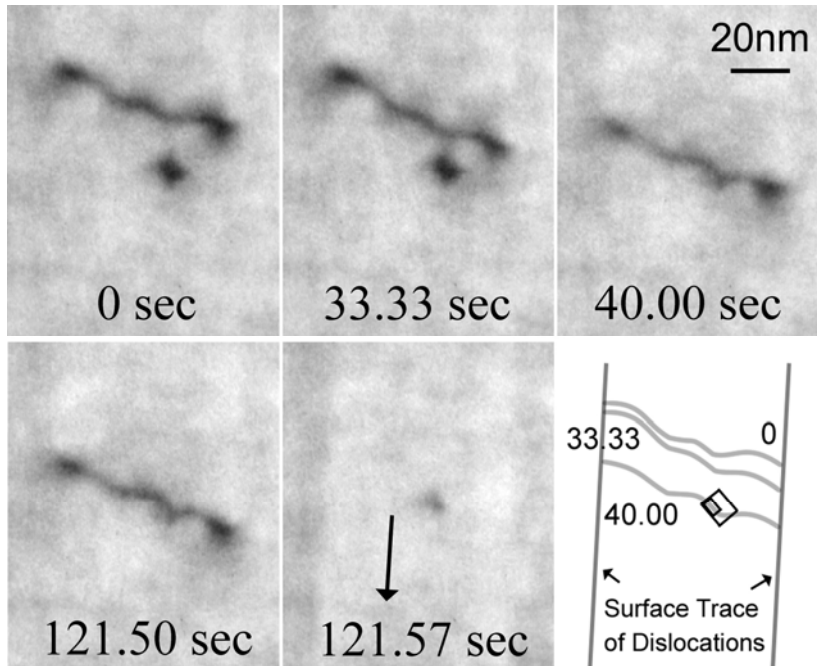


Fig. 10. Same SFT destruction process as Fig. 9. The original SFT size and the remnant apex portion were 11 and 5 nm, respectively. The schematic diagram shown in the lower right is the trace of the gliding dislocation in each frame. After the SFT destruction, the dislocation continued to glide on the same slip plane as before.

In the present in situ deformation study, the velocity of dislocation motion was roughly $10^{-8}\sim 10^{-7}$ m/s [35], which is significantly slower than the dislocation velocity in MD simulations ($10^1\sim 10^3$ m/s [26,28]). The significant difference in the dislocation velocity is a conceivable factor causing the discrepancy in results. Another conceivable factor is the effect of non-uniform deformation in the TEM specimens. As addressed in detail in the Appendix section, the stress state in the non-uniformly deforming specimens may be multiaxial. Pure uniaxial stress conditions applied in MD simulations would be more favorable for double cross-slip.

To date the Kimura process has never been confirmed in MD simulations, whereas our TEM observation revealed that the Kimura process (for a screw dislocation) can occur for small SFTs within the size range reproducible in MD simulations. The reason for this discrepancy is unclear. The SFT size range where processes (3.1) and (3.3) were observed in the present study overlaps each other: both of them were observed at all SFT sizes (10~50 nm). Therefore, the SFT size is not the crucial factor distinguishing these two processes. As confirmed in the present TEM study, the Kimura process for a screw dislocation was induced when the screw dislocation impinged on the SFT near the base triangle. This is a possible key point to distinguish process (3.1) from (3.3). However, in MD simulations the Kimura process was not reproduced even when the dislocation impinged the SFT at the base triangle [30]. The complexity of the stress state mentioned above is therefore the remaining major factor causing the absence of the Kimura process in MD simulations.

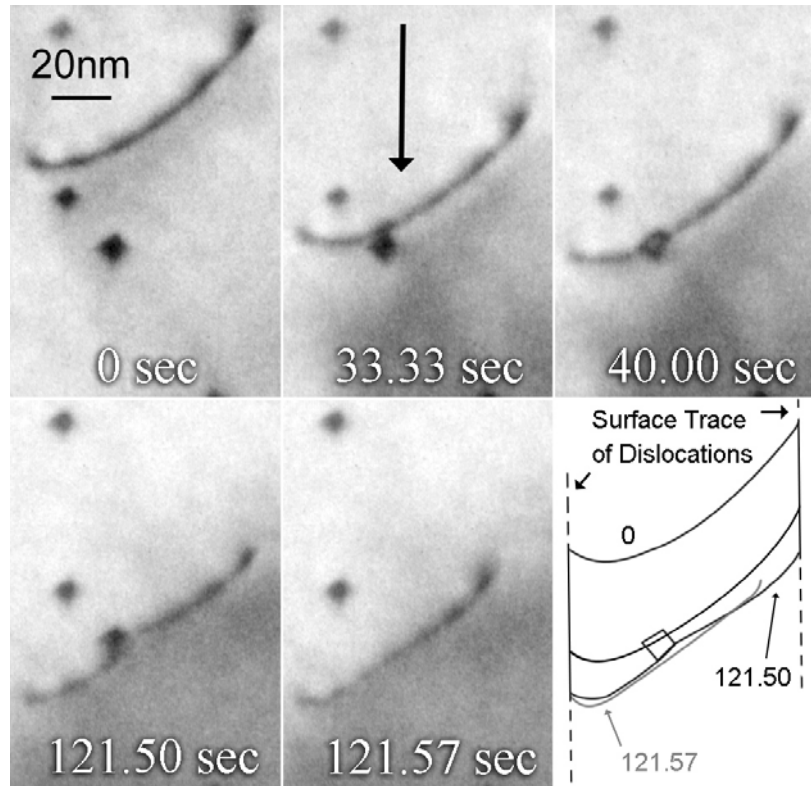


Fig. 11. SFT destruction process leaving behind no remnants and no sessile segments on the dislocation. The SFT size was 11 nm. The schematic diagram shown in the lower right is the trace of the gliding dislocation in each frame. The dislocation cross-slipped upon SFT annihilation.

Conclusions

We confirmed the following four SFT destruction processes by incident dislocations.

(1) *Kimura process* - We observed SFT destruction processes consistent with the Kimura model for both screw and 60-degree dislocations [25]: i.e. the processes that leave multiple super jog segments on the gliding dislocation (for screw) and a triangular Frank loop (for 60-degree). For screw dislocations this was confirmed in a wide SFT size range (10~50 nm). These TEM observations support the validity of the Kimura model. To date the Kimura process has not been reproduced in limited MD simulations, whereas the Kimura process for a screw dislocation was experimentally confirmed for SFTs as small as ~10 nm.

(2) *Stress-induced SFT collapse* - This was the dominant destruction process for large SFTs (>34 nm) when interacting with the leading dislocation in a dislocation queue (dislocation pile-up). Since such large SFTs are meta-stable [5,40], they favor a collapse into a triangular Frank loop via an inverse Silcox and Hirsch or a related mechanism [1] with the aid of high stress at the pile-up front. This collapse process is similar to Kimura's model for a 60-degree dislocation in terms of the remnant type but different in the position (habit plane) where the Frank loop forms.

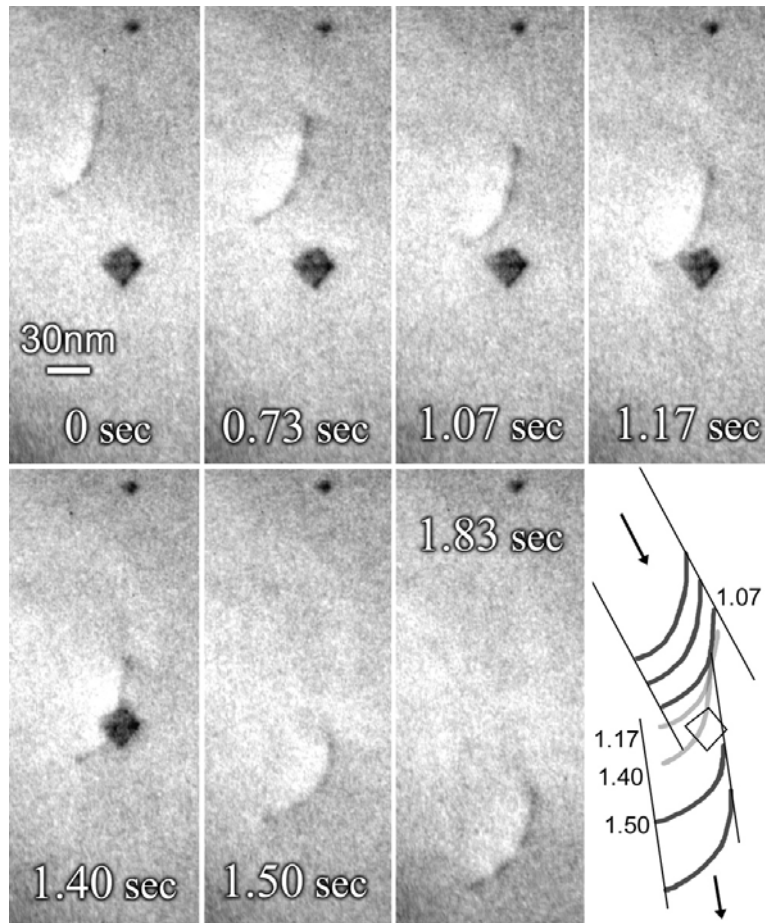


Fig. 12. Same SFT destruction process as Fig. 11 but observed at 873K. The SFT size was 30 nm. The schematic diagram shown in the lower right is the trace of the gliding dislocation in each frame.

(3) *Partial SFT annihilation leaving an apex portion* – It appears as though this is essentially the same process as recent MD models. This process was confirmed at all SFT sizes (10~50 nm). Occasionally, sessile segments were formed on the impinging dislocation (super jogs on a screw dislocation). However, the dislocation released those sessile segments through the interaction with other gliding dislocations. The dislocation that released the sessile segments was then mobile.

(4) *Complete SFT annihilation without any remnants* – This process was observed only for small SFTs (~10 nm) at room temperature; however, at high temperature (~873K) this process was induced for larger SFTs (~30 nm) as well. When this process was induced, the gliding dislocation always cross-slipped, indicating that this process can be induced only by screw dislocations.

Acknowledgements

This research was sponsored by Office of Fusion Energy Sciences, U.S. Department of Energy, under contract DE-ACO5-00OR22725 with UT-Battelle, LLC. We thank Dr. Thak Sang Byun for valuable comments.

References

- [1] J. Silcox and P. B. Hirsch, *Philos. Mag.* 4 (1959) 72.
- [2] S. Kojima, Y. Satoh, H. Taoka, I. Ishida, T. Yoshiie, and M. Kiritani, *Philos. Mag. A* 59 (1989) 519.
- [3] M. Kiritani, *Mater. Chem. Phys.* 50 (1997) 133.
- [4] R. E. Smallman and K. H. Westmacott, *Mater. Sci. Eng.* 9 (1972) 249.
- [5] S. J. Zinkle, L. E. Seitzman, and W. G. Wolfer, *Philos. Mag. A* 55 (1987) 111.
- [6] M. Kiritani, *J. Nucl. Mater.* 216 (1994) 220.
- [7] H. Watanabe, T. Muroga, and N. Yoshida, *J. Nucl. Mater.* 217(1-2) (1994) 178.
- [8] Y. Dai, X. Jia, J. C. Chen, W. F. Sommer, M. Victoria, and G. S. Bauer, *J. Nucl. Mater.* 296 (2001) 174.
- [9] M. Victoria, N. Baluc, C. Baliai, Y. Dai, M. I. Luppó, R. Schaublin, and B. N. Singh, *J. Nucl. Mater.* 276 (2000) 114.
- [10] B. N. Singh, *Encyclopedia of Materials: Science and Technology*, K. H. J. Buschow et al. (eds.), Elsevier Science Ltd., ISBN: 0-08-0431526 (2001) 7957.
- [11] B. N. Singh, S. I. Golubov, H. Trinkaus, D. J. Edwards, and M. Eldrup, *J. Nucl. Mater.* 328 (2004) 77.
- [12] M. Meshii and J. W. Kauffman, *Acta Metall.* 7 (1959) 180.
- [13] M. S. Bapna, T. Mori, and M. Meshii, *Philos. Mag.* 17 (1968) 177.
- [14] S. Yoshida, M. Kiritani, Y. Deguchi, and N. Kamigaki, *Mater. Trans. JIM* 9 (supplement) (1968) 89.
- [15] A. Okada, K. Kanao, T. Yoshiie, and S. Kojima, *Mater. Trans. JIM* 30 (1989) 265.
- [16] S. J. Zinkle, *Radiat. Eff. Defects Solids* 148 (1999) 447.
- [17] N. Ajita, H. Hashimoto, and Y. Takaki, *Phys. Stat. Sol. (a)* 87 (1985) 235.
- [18] J. V. Sharp, *Philos. Mag.* 16 (1967) 77.
- [19] H. Saka, K. Noda, K. Matsumoto, and T. Imura, *Proceedings of 4th International Conference on High Voltage Electron Microscopy, Toulouse (1975)* 325.
- [20] K. Noda, H. Saka, K. Shiraishi, H. Yoshida, and T. Imura, *Proceedings of 5th International Conference on High Voltage Electron Microscopy, Kyoto (1977)* 403.
- [21] E. Johnson and P. B. Hirsch, *Philos. Mag. A* 43 (1981) 157.
- [22] J. S. Robach, I. M. Robertson, B. D. Wirth, and A. Arsenlis, *Philos. Mag.* 83 (2003) 955.
- [23] L. Z. Sun, N. M. Ghoniem, and Z. Q. Wang, *Mater. Sci. Eng. A* 309-310 (2001) 178.
- [24] M. Hiratani, H. M. Zbib, and B. D. Wirth, *Philos. Mag. A* 82, No.14 (2002) 2709.
- [25] H. Kimura and R. Maddin, *Lattice Defects in Quenched Metals*, *Proceedings of an International Conference*, Argonne National Laboratory, R. M. J. Cotterill (ed.), Academic Press, New York (1965) 319.
- [26] B. D. Wirth, V. V. Bulatov, and T. D. de la Rubia, *J. Eng. Mater. Technol.* 124 (2002) 329.
- [27] Y. N. Osetsky, D. J. Bacon, B. N. Singh, and B. D. Wirth, *J. Nucl. Mater.* 307-311 (2002) 852.
- [28] Y. N. Osetsky, R. E. Stoller, and Y. Matsukawa, *J. Nucl. Mater.* 329-333 (2004) 1228.
- [29] Y. N. Osetsky, R. E. Stoller, D. Rodney, and D. J. Bacon, *Mater. Sci. Eng. A* 400 (2005) 370.
- [30] Y. N. Osetsky, D. Rodney, and D. J. Bacon, *Philos. Mag.* 86, No. 16 (2006) 2295.
- [31] Y. N. Osetsky, R. E. Stoller, Y. Matsukawa, and S. J. Zinkle, *Philos. Mag. Lett.* 86 (2006) 511.
- [32] Y. Matsukawa and S. J. Zinkle, *J. Nucl. Mater.* 329-333 (2004) 919.
- [33] S. J. Zinkle and Y. Matsukawa, *J. Nucl. Mater.* 329-333 (2004) 88.
- [34] Y. Matsukawa, Y. N. Osetsky, R. E. Stoller, and S. J. Zinkle, *Mater. Sci. Eng. A* 400 (2005) 366.
- [35] Y. Matsukawa, Y. N. Osetsky, R. E. Stoller, and S. J. Zinkle, *J. Nucl. Mater.* 351 (2006) 285.
- [36] R. Schaublin, Z. Yao, P. Spatig, and M. Victoria, *Mater. Sci. Eng. A* 400 (2005) 251.
- [37] J. S. Robach, I. M. Robertson, H.-J. Lee, and B. D. Wirth, *Acta Mater.* 54 (2006) 1679.
- [38] N. M. Ghoniem, S.-H. Tong, B. N. Singh, and L. Z. Sun, *Philos. Mag. A* 81, No. 11 (2001) 2743.
- [39] T. D. de la Rubia, H. M. Zbib, T. A. Khraishi, B. D. Wirth, M. Victoria, and M. Caturla, *Nature* 406, No. 6798 (2000) 871-874.

- [40] T. Jøssang and J. P. Hirth, *Philos. Mag.* 13 (1966) 657.
- [41] G. Thomas and J. Washburn, *Rev. of Modern Phys.* 35, No. 4 (1963) 992.
- [42] L. M. Clarebrough, R. L. Segall, M. H. Loretto, and M. E. Hargreaves, *Philos. Mag.* 9 (1964) 377.
- [43] R. L. Segall and L. M. Clarebrough, *Philos. Mag.* 9 (1964) 865.
- [44] I. A. Johnston, P. S. Dobson, and R. E. Smallman, *Cryst. Lattice Defects* 2 (1971) 127.
- [45] J. P. Hirth and J. Lothe, *Theory of Dislocation*, Second Edition, McGraw-Hill, New York, 1982.
- [46] V. R. Parameswaran, N. Urabe, and J. Weertman, *J. Appl. Phys.* 43, No. 7 (1972) 2982.
- [47] W. F. Greenman, T. Vreeland, Jr., and D. S. Wood, *J. Appl. Phys.* 38, No. 9 (1967) 3595.
- [48] Y. N. Osetsky, *Philos. Mag.* 83 (2003) 3623.
- [49] T. Hatano and H. Matsui, *Phys. Rev. B* 72, No. 9 (2005) 094105.
- [50] K. Nogiwa, T. Yamamoto, K. Fukumoto, Y. Nagai, K. Yubuta, and M. Hasegawa, *J. Nucl. Mater.* 307, Part B (2002) 946.